molecules

MDPI

Article

The *Cis*-Effect Explained Using Next-Generation QTAIM

Yuting Peng [1], Wenjing Yu [1], Xinxin Feng [1], Tianlv Xu [1], Herbert Früchtl [2], Tanja van Mourik [2], Steven R. Kirk [1,*] and Samantha Jenkins [1,*]

[1] Key Laboratory of Chemical Biology and Traditional Chinese Medicine Research and Key Laboratory of Resource National and Local Joint Engineering Laboratory for New Petro-chemical Materials and Fine Utilization of Resources, College of Chemistry and Chemical Engineering, Hunan Normal University, Changsha 410081, China

[2] EaStCHEM School of Chemistry, University of St Andrews, North Haugh, St Andrews, Fife KY16 9ST, Scotland, UK

* Correspondence: steven.kirk@cantab.net (S.R.K.); samanthajsuman@gmail.com (S.J.)

Abstract: We used next-generation QTAIM (NG-QTAIM) to explain the *cis*-effect for two families of molecules: C_2X_2 (X = H, F, Cl) and N_2X_2 (X = H, F, Cl). We explained why the *cis*-effect is the exception rather than the rule. This was undertaken by tracking the motion of the bond critical point (*BCP*) of the stress tensor trajectories $T_\sigma(s)$ used to sample the U_σ-space cis- and trans-characteristics. The T_σ(s) were constructed by subjecting the C1-C2 BCP and N1-N2 BCP to torsions ± θ and summing all possible T_σ(s) from the bonding environment. During this process, care was taken to fully account for multi-reference effects. We associated bond-bending and bond-twisting components of the T_σ(s) with *cis*- and *trans*-characteristics, respectively, based on the relative ease of motion of the electronic charge density $\rho(\mathbf{r_b})$. Qualitative agreement is found with existing experimental data and predictions are made where experimental data is not available.

Keywords: QTAIM; NG-QTAIM; cis-effect; dihaloethene; dihalodiazene

Citation: Peng, Y.; Yu, W.; Feng, X.; Xu, T.; Früchtl, H.; van Mourik, T.; Kirk, S.R.; Jenkins, S. The *Cis*-Effect Explained Using Next-Generation QTAIM. *Molecules* **2022**, *27*, 6099. https://doi.org/10.3390/molecules27186099

Academic Editor: Rudy J. Richardson

Received: 10 August 2022
Accepted: 14 September 2022
Published: 18 September 2022

1. Introduction

An extensive body of literature exists on the subject of the *cis*-effect over the last 40 years, on the basis of both theory [1–6] and experiment [6–17]. The *cis*-effect is a phenomenon in which the *cis*-isomer is more stable than [2,4,7–9] or, in molecules with double bonds, almost as energetically stable as the corresponding *trans*-isomer. Computational results of the relative energy differences of the *cis*- and *trans*-isomers are compared with existing experimental data [7–16] that in some cases suffer from large uncertainties in the measurements [7,15–17]. In this study, we will not use energy-based approaches to attempt to understand the mechanism of the *cis*-effect; instead, we will use an electronic charge-density-based analysis.

Earlier, some of the current authors provided a *scalar* physics-inspired coupling mechanism explaining the *cis*-effect in terms of electronic and nuclear degrees of freedom for three families of molecules, including halogen-substituted ethene and diazenes [18]. We undertook a *static* investigation of the properties of the central X = X or N = N bond paths and found that those of the *cis*-isomers were more bent: the difference between the length of the bond path and the internuclear separation was up to 1.5% larger in the *cis*-isomers than in the corresponding *trans*-isomers. In our earlier contribution, we therefore concluded that the physical origin of the *cis*-effect was associated with greater bond-path bending. This earlier work, however, only provided correlations of the bond-path bending with the energy and did not explain why the *cis*-effect is the exception rather than the rule. In this work, the physical basis of the *cis*-effect will be provided in terms of the least and most preferred directions of electronic charge density motion.

Recently, some of the current authors used an electronic charge-density-based analysis to investigate steric effects within the formulation of next-generation Quantum Theory of

Atoms in Molecules (NG-QTAIM) [19]. We found that the presence of chiral contributions suggested that steric effects, rather than hyperconjugation, explained the staggered geometry of ethane [20]. This recent work on steric effects relates to the current investigation on cis-effects, since in both cases we subject the central C = C or N = N bond to a torsion to probe either steric or *cis*-effects. Low/high values of the NG-QTAIM interpretation of chirality (C_σ) were associated with low/high steric effects due to the absence/presence of an asymmetry. The chirality C_σ [21] was earlier used to redefine a related quantity for cumulenes, the bond-twist T_σ [22].

In this investigation, we will use NG-QTAIM to explain why the *cis*-effect was previously found, in our scalar investigation, to be associated with bond bending [18]. This will be undertaken by subjecting the axial bonds, C1-C2 and N1-N2, to a torsion θ to sample the directional response of the electronic charge density $\rho(\mathbf{r_b})$ at the bond cross-section. This will provide a better understanding of the greater (topological) stability of the *cis*-isomer over the *trans*-isomer in these halogen-containing species; see Scheme 1.

Scheme 1. In-plane views of the *cis*- and *trans*-isomers for substitutions of the ethene (left panel) and diazene (right panel) molecular graphs, where X3 = X6 = H, F, Cl. The atomic numbering scheme of the four substituted ethene isomers for the *cis*- (X3-C1-C2-X6, X3-C1-C2-H5, H4-C1-C2-H5, H4-C1-C2-X6) and *trans*-isomers (X4-C1-C2-X6, X4-C1-C2-H5, H3-C1-C2-H5, H3-C1-C2-X6). The dihedral X3-**N1-N2**-X4 is used for the *cis*- and *trans*-isomers of the diazenes. The undecorated green spheres indicate the locations of the bond critical points (*BCP*s).

2. Theoretical Background and Computational Details

2.1. Theoretical Background

The QTAIM and next-generation QTAIM (NG-QTAIM) [23–29] background is provided in the Supplementary Materials S1, including the procedure to generate the stress tensor trajectories $T_\sigma(s)$.

We use Bader's formulation of the quantum stress tensor σ(r) [30] to characterize the forces on the electron density distribution in open systems that is defined by:

$$\sigma(\mathrm{r}) = -\frac{1}{4}\left[\left(\frac{\partial^2}{\partial \mathrm{r}_i \partial \mathrm{r}'_j} + \frac{\partial^2}{\partial \mathrm{r}'_i \partial \mathrm{r}_j} - \frac{\partial^2}{\partial \mathrm{r}_i \partial \mathrm{r}_j} - \frac{\partial^2}{\partial \mathrm{r}'_i \partial \mathrm{r}'_j}\right)\cdot\gamma(\mathrm{r},\mathrm{r}')\right]_{\mathrm{r}=\mathrm{r}'} \quad (1)$$

where $\gamma(\mathbf{r},\mathbf{r}')$ is the one-body density matrix,

$$\gamma(\mathrm{r},\mathrm{r}') = N\int \Psi(\mathrm{r},\mathrm{r}_2,\ldots,\mathrm{r}_N)\Psi^*(\mathrm{r}',\mathrm{r}_2,\ldots,\mathrm{r}_N)\mathrm{d}\mathrm{r}_2\cdots\mathrm{d}\mathrm{r}_N \quad (2)$$

The stress tensor is then any quantity σ(r) that can satisfy equation (2): any divergence-free tensor can be added [30–32]. Bader's formulation of the stress tensor σ(r), equation (1), is a standard option in the AIMAll QTAIM package [33]. Earlier Bader's formulation of σ(r) demonstrated superior performance compared with the Hessian of ρ(r) for distinguishing the S_a- and R_a-geometric stereoisomers of lactic acid [34] and therefore will be used in this investigation.

In this investigation, we include the entire bonding environment, including all contributions to the U_σ-space *cis*- and *trans*-characteristics, by considering the C1-C2 *BCP* $T_\sigma(s)$

of the asymmetric, i.e., 'reference' carbon atom (C1) or the N1-N2 BCP $T_\sigma(s)$ of the nitrogen atom (N1); see Scheme 1 and the Computational Details section. The C1-C2 *BCP* $T_\sigma(s)$ and N1-N2 BCP $T_\sigma(s)$ are created by subjecting these BCP bond paths to a set of torsions θ; see the Computational Details section.

The bond-twist T_σ is the difference in the maximum projections, the dot product of the stress tensor $e_{1\sigma}$ eigenvector and the BCP displacement dr, of the $T_\sigma(s)$ values between the counter-clockwise (CCW) and clockwise (CW) torsion θ.

$$T_\sigma = [(e_{1\sigma}\cdot dr)_{max}]_{CCW} - [(e_{1\sigma}\cdot dr)_{max}]_{CW} \quad (3)$$

Equation (3) for the bond-twist T_σ quantifies the bond torsion *BCP*-induced *bond twist* for the CCW vs. CW direction, where the largest magnitude stress tensor eigenvalue ($\lambda_{1\sigma}$) is associated with $e_{1\sigma}$; see Figures 1 and 2. The eigenvector $e_{1\sigma}$ corresponds to the direction along which electrons at the *BCP* are subject to the most compressive forces. Therefore, $e_{1\sigma}$ corresponds to the direction along which the *BCP* electrons will be displaced most readily when the *BCP* is subjected to a torsion [35]. Higher values of the bond twist T_σ correspond to greater asymmetry, and therefore to a dominance of the *trans*- compared with the *cis*-isomer in U_σ space. This reflects the structural symmetry, with respect to the positioning of the halogen substituents, of the *trans*- rather than the *cis*-isomer.

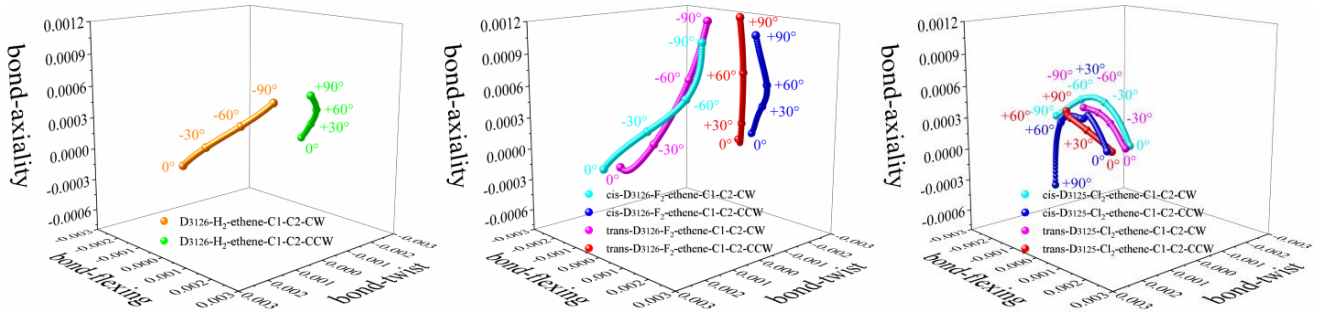

(a) **(b)** **(c)**

Figure 1. The torsion C1-C2 *BCP* stress tensor trajectories $T_\sigma(s)$ for the Cartesian clockwise (CW) and counter-clockwise (CCW) torsion directions for the geometric *cis*- and *trans*-isomers of H_2-ethene, F_2-ethene and Cl_2-ethene are presented in sub-figures (**a**–**c**), respectively; see Table 1. Notice the markers at 30° intervals.

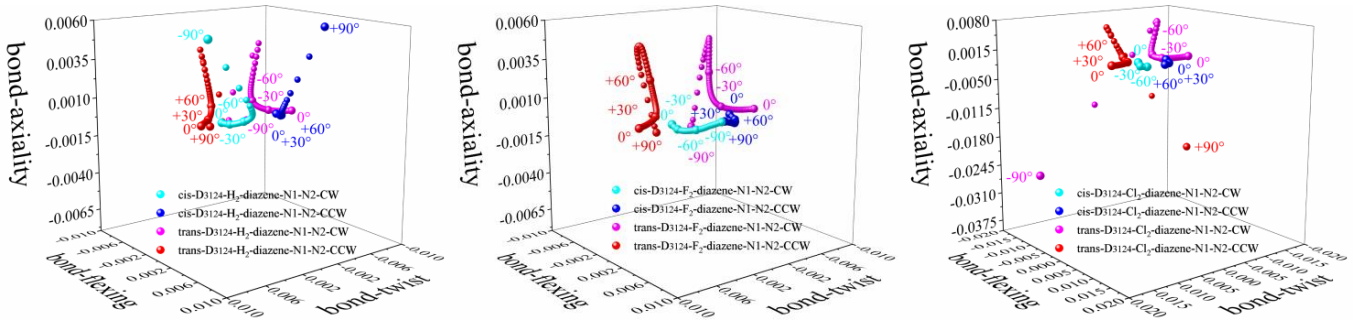

(a) **(b)** **(c)**

Figure 2. The N1-N2 *BCP* stress tensor trajectories $T_\sigma(s)$ for the Cartesian CW and CCW torsions for the *cis*- and *trans*-isomers of H_2-diazene, F_2-diazene and Cl_2-diazene are presented in sub-figures (**a**–**c**), respectively; see the caption of Figure 1 and Table 2.

Table 1. The U_σ-space bond cross-section sets {bond-twist T_σ, bond-flexing F_σ} of the torsion C1-C2 BCP, and the sum $\sum\{T_\sigma,F_\sigma\}$, of ethene and the cis- and trans-isomers of doubly substituted ethene. The atom numbering sequence for the dihedral angles used to construct the T_σ(s) is indicated by the four-digit sequence (left column); see Scheme 1.

	$\{T_\sigma, F_\sigma\}$	
	H_2	
D_{3125}	$\{-0.00096[R_\sigma], 0.00023[S_\sigma]\}$	
D_{3126}	$\{0.00003[S_\sigma], 0.00006[S_\sigma]\}$	
D_{4125}	$\{0.00560[S_\sigma], 0.00013[S_\sigma]\}$	
D_{4126}	$\{0.00017[S_\sigma], -0.00012[R_\sigma]\}$	
	$\sum\{T_\sigma, F_\sigma\}$	
	$\{0.00483[S_\sigma], 0.00030[S_\sigma]\}$	
	cis-ethene	*trans-ethene*
	$\{T_\sigma, F_\sigma\}$	$\{T_\sigma, F_\sigma\}$
	F_2	
D_{3125}	$\{0.00056[S_\sigma], -0.00190[R_\sigma]\}$	$\{0.01731[R_\sigma], 0.00000[Q_\sigma]\}$
D_{3126}	$\{-0.01339[R_\sigma], 0.00004[S_\sigma]\}$	$\{0.00111[S_\sigma], 0.00026[S_\sigma]\}$
D_{4125}	$\{0.00002[S_\sigma], -0.00149[R_\sigma]\}$	$\{-0.00030[R_\sigma], 0.00028[S_\sigma]\}$
D_{4126}	$\{0.00143[S_\sigma], -0.00158[R_\sigma]\}$	$\{-0.00060[R_\sigma], -0.00011[R_\sigma]\}$
	$\sum\{T_\sigma, F_\sigma\}$	$\sum\{T_\sigma, F_\sigma\}$
	$\{-0.01138[R_\sigma], -0.00493[R_\sigma]\}$	$\{-0.01710[R_\sigma], 0.00043[S_\sigma]\}$
	Cl_2	
D_{3125}	$\{0.14080[S_\sigma], 0.95259[S_\sigma]\}$	$\{0.00009[S_\sigma], 0.00022[S_\sigma]\}$
D_{3126}	$\{-0.00093[R_\sigma], 0.00088[S_\sigma]\}$	$\{-0.40475[R_\sigma], 0.19420[S_\sigma]\}$
D_{4125}	$\{-0.00093[R_\sigma], -0.00001[R_\sigma]\}$	$\{0.00017[S_\sigma], -0.00091[R_\sigma]\}$
D_{4126}	$\{-0.38727[R_\sigma], 0.11232[S_\sigma]\}$	$\{0.00033[S_\sigma], 0.00001[S_\sigma]\}$
	$\sum\{T_\sigma, F_\sigma\}$	$\sum\{T_\sigma, F_\sigma\}$
	$\{-0.24833[R_\sigma], 1.06578[S_\sigma]\}$	$\{-0.40417[R_\sigma], 0.19351[S_\sigma]\}$

Table 2. The U_σ-space bond cross-section sets $\{T_\sigma,F_\sigma\}$ of the C1-C2 *BCP* for the doubly substituted diazene torsion.

cis-diazene	*trans*-diazene
$\{T_\sigma, F_\sigma\}$	$\{T_\sigma, F_\sigma\}$
H_2	
$\{0.00812[S_\sigma], 0.00016[S_\sigma]\}$	$\{-0.00176[R_\sigma]\}, \{0.00070[S_\sigma]\}$
F_2	
$\{-0.01077[R_\sigma], -0.00886[R_\sigma]\}$	$\{0.00023[S_\sigma]\}, \{0.00014[S_\sigma]\}$
Cl_2	
$\{0.00020[S_\sigma], 0.00672[S_\sigma]\}$	$\{-0.00022[R_\sigma]\}, \{-0.00402[R_\sigma]\}$

Conversely, the eigenvector $e_{2\sigma}$ corresponds to the direction along which the electrons at the *BCP* are subject to the least compressive forces. Therefore, $\mathbf{e_{2\sigma}}$ corresponds to the direction along which the *BCP* electrons will be least readily displaced when the *BCP* undergoes a torsion distortion. The *bond-flexing* F_σ associated with $\mathbf{e_{2\sigma}}$ is defined as:

$$F_\sigma = [(e_{2\sigma}\cdot dr)_{max}]_{CCW} - [(e_{2\sigma}\cdot dr)_{max}]_{CW} \quad (4)$$

The bond-flexing F_σ is calculated from the torsion *BCP bond flexing* defined by equation (4); see Figures 1 and 2. Equation (4) provides a U_σ-space measure of the 'flexing-strain' or bond bending that a bond path is under in the *cis*- or *trans*-isomer configurations. This is consistent with greater 'flexing-strain' or bond bending that previously correlated with a greater presence of the *cis*-effect [18]. Higher values of F_σ correspond to the dominance of the *cis*- compared with the *trans*-isomer in U_σ space, because bond bending reflects the symmetry of the *cis*-isomer rather than the *trans*-isomer, with respect to the positioning of the halogen substituents.

The bond-axiality A_σ is part of the U_σ-space distortion set $\sum\{T_\sigma,F_\sigma,A_\sigma\}$, which provides a measure of the chiral asymmetry. It is defined as:

$$A_\sigma = [(e_{3\sigma}\cdot dr)_{max}]_{CCW} - [(e_{3\sigma}\cdot dr)_{max}]_{CW} \quad (5)$$

Equation (5) quantifies the direction of *axial* displacement of the bond critical point (*BCP*) in response to the bond torsion (CCW vs. CW), i.e., the sliding of the *BCP* along the bond path. We will, however, not use A_σ as it does not comprise the bond cross-section, but provide it in the Supplementary Materials S5 and S6. Instead, we will use the so-called U_σ-space *bond cross-section* set $\sum\{T_\sigma,F_\sigma\}$ developed for *cis*- and *trans*-isomers.

The (+/−) sign of the bond-twist T_σ and bond-flexing F_σ determines the S_σ ($T_\sigma > 0$, $F_\sigma > 0$) or R_σ ($T_\sigma < 0$, $F_\sigma < 0$) character; see Tables 1 and 2.

The bond cross-section set $\sum\{T_\sigma,F_\sigma\}$ is related to the cross-section of a *BCP* bond path that is quantified by the $\lambda_{1\sigma}$ and $\lambda_{2\sigma}$ eigenvalues associated with the $e_{1\sigma}$ and $e_{2\sigma}$ eigenvectors, respectively. Note, the $e_{1\sigma}$ and $e_{2\sigma}$ eigenvectors are the directions along which the *BCP* electrons are displaced most readily and least readily, respectively, when the *BCP* is subject to a torsional distortion. The *trans*-isomer is dominant in U_σ space if the magnitude of the bond-twist T_σ value is larger for the *trans*- than for the *cis*-isomer. Conversely, dominance of the *cis*-isomer is determined by the presence of a larger magnitude bond-flexing F_σ value for the *cis*-isomer compared with the *trans*-isomer; see Tables 1 and 2.

2.2. Computational Details

The electronic wavefunction for molecular structures incorporating a chemically conventional double bond is usually well-represented by a single-reference wavefunction in the 'eclipsed' configurations 0° (*cis*) or 180° (*trans*). It is also well-known that as the dihedral angle across the double bond deviates from the 'eclipsed' configurations, the nature of the wavefunction changes, becoming fully multi-reference in nature at the twisted 90° 'staggered' configuration. The multi-reference character is determined for ethene using the frequently used T1 measure [36], where values of T1 > 0.02 indicate that a single-reference description is inadequate. For this reason, in all of this work, for both the C_2X_2 (X = H, F, Cl) and N_2X_2 (X = H, F, Cl) molecules, we use a multi-reference CAS-SCF(2,2) method [37,38], using Slater determinants for the active space, implemented in Gaussian G09.E01 [39] with symmetry disabled, an 'ultrafine' integration grid and convergence criteria of 'VeryTight' geometry convergence and an SCF convergence criterion of 10^{-12}. The cc-pVTZ triple-zeta basis set was used during geometry optimization and the dihedral coordinate scan constrained geometry optimization process. The magnitude of the dihedral angle scan steps was 1°. Additionally, the second atom used in each sequence defining the dihedral scan angle, C1 and N1, respectively, for the ethene and diazene derivatives, was constrained to be fixed at the origin of the Cartesian spatial coordinates. All initial 'eclipsed' (*cis*- and *trans*-) optimized molecular geometries were generated (and checked to be energy minima with no imaginary vibrational frequencies) with these settings; see Supplementary Materials S2 for the optimized structures and tabulated experimental data. The final single-point wavefunctions and densities for each structure produced during the dihedral scans were calculated, as recommended for accurate NG-QTAIM properties [40], using a quadruple-zeta basis set (cc-pVQZ).

The direction of torsion is determined to be CCW ($0.0° \leq \theta \leq +90.0°$) or CW ($-90.0° \leq \theta \leq 0.0°$) from an increase or a decrease in the dihedral angle, respectively. An exception is made for

N_2Cl_2 where the respective angular limits used were −80° and +80°. These latter limits are chosen due to the well-known destabilizing interactions between the nitrogen lone pairs and the relatively weak N-Cl bonds [41,42], which cause dissociation of the molecule into N_2 and Cl_2 when a larger twist is applied: we observed and confirmed this dissociation for dihedral twists > 80°.

The stress tensor trajectories $T_\sigma(s)$ for all four of the possible ordered sets of four atoms that define the dihedral angle for each of the *cis*-isomers (X3-C1-C2-X6, X3-C1-C2-H5, H4-C1-C2-H5, H4-C1-C2-X6) and *trans*-isomers (X4-C1-C2-X6, X4-C1-C2-H5, H3-C1-C2-H5, H3-C1-C2-X6) are calculated; see the left panel of Scheme 1 for the dihedral atom numbering. There is a single dihedral X3-N1-N2-X4 for each of the *cis*- and *trans*-isomers of the diazenes N_2X_2 (X = H, F, Cl); see the right panel of Scheme 1.

QTAIM and stress tensor analysis were then performed on each single-point wavefunction obtained in the previous step with the AIMAll [33] and QuantVec [43] suite. In addition, all molecular graphs were confirmed to be free of non-nuclear attractor critical points.

3. Results and Discussions

The scalar distance measures geometric bond length (GBL) and bond path length (BPL) used in this investigation on ethene, doubly substituted ethene and diazene are insufficient to quantify the presence of the *cis*-effect and are provided in the Supplementary Materials S3. The variation in the (scalar) relative energy ΔE for ethene, doubly substituted ethene and diazene molecules do not provide any insights either into the *cis*-effect for these molecules and are provided in the Supplementary Materials S4. The intermediate and the complete C1-C2 *BCP* U_σ-space distortion sets are provided in the Supplementary Materials S5 and S6, respectively.

The sum of the bond-cross-section sets $\sum\{T_\sigma,F_\sigma\}$ of the C1-C2 *BCP* $T_\sigma(s)$ was calculated for all four possible isomers of the formally achiral molecules ethene and doubly substituted ethane, C_2X_2 (X = H, F, Cl). The results for the molecular graph of pure ethene are provided as a control to enable a better understanding of the effect of the halogen atom substitutions; see Table 1 and Scheme 1. The corresponding results for the formally achiral diazenes N_2X_2 (X = H, F, Cl) comprising a single isomer N1-N2 *BCP* $T_\sigma(s)$ are presented in Table 2. The magnitude of the values of the bond cross-section set $\sum\{T_\sigma,F_\sigma\}$ increases with atomic weight, as is demonstrated for F_2 and Cl_2 substitution of ethene; see Table 1. This relationship between the magnitude of the $\sum\{T_\sigma,F_\sigma\}$ values and halogen substituent also occurred in a recent investigation of singly and doubly halogen-substituted ethane [44]. This dependency of $\{T_\sigma,F_\sigma\}$ on the atomic weight of the substituent, however, does not occur for the diazenes.

The magnitude of the bond-twist T_σ is significantly smaller for the *cis*- compared with the *trans*-isomer for C_2X_2 (X = F, Cl) and slightly smaller for N_2X_2 (X = Cl). The magnitude of the bond-flexing F_σ is significantly larger for the *cis*- compared with the *trans*-isomer for C_2X_2 (X = F, Cl) and N_2X_2 (X = F, Cl).

These results for the bond cross-section set $\sum\{T_\sigma,F_\sigma\}$ are consistent with the presence of the *cis*-effect and therefore indicate the occurrence of the *cis*-effect in U_σ space for C_2X_2 (X = F, Cl) and N_2X_2 (X = F, Cl). The very large component of the bond-twist T_σ for N_2X_2 (X = H) indicates a complete lack of the *cis*-effect and a dominance of the *trans*-isomer in U_σ space for this molecule.

All of the investigated molecular graphs comprised a significant degree of chiral character as indicated by the magnitudes of the bond-twist T_σ and bond-flexing F_σ, particularly for C_2X_2 (X = F, Cl).

4. Conclusions

In this investigation, NG-QTAIM was used to determine the presence or absence of the *cis*-effect for the C_2X_2 (X = H, F, Cl) and N_2X_2 (X = H, F, Cl) molecules. Qualitative agreement with experimental data for differences in the energies of the *cis*- and *trans*-isomers was found.

The molecules of this investigation are formally achiral according to the Cahn–Ingold–Prelog (CIP) priority rules [45], but all comprise at least a degree of chiral character in U_σ space, on the basis of the magnitude of the T_σ values, with C_2X_2 (X = Cl) displaying a very significant degree of chirality. This finding reflects the conventional understanding that steric effects are among the reasons for the differences between the relative energetic stabilities of *cis*- and *trans*-isomers, consistent with our previous association of chiral character in Uσ space for the steric effects for ethane [20].

We found that both C_2X_2 (X = F, Cl) and N_2X_2 (X = F, Cl) display the *cis*-effect. This includes the prediction of a cis-effect in N_2X_2 (X = Cl), for which no experimental data on the *cis*-isomer and *trans*-isomer energy difference are available. The *cis*-effect is determined on the basis of the much larger values of the bond-flexing Fσ for the *cis*- compared with the *trans*-isomer.

We provided a physical explanation as to why the *cis*-effect is the exception rather than the rule, by defining a dominant bond-flexing F_σ component of the bond cross-section set $\{T_\sigma,F_\sigma\}$ as characterizing the *cis*-effect. This is on the basis that it is more difficult to bend (F_σ) than to twist (T_σ) the C1-C2 *BCP* bond path and N1-N2 *BCP* bond path. This difference in the difficulty of performing bond-bending (F_σ) and bond-twisting (T_σ) distortions is explained by their construction, using the least preferred $e_{2\sigma}$ and most preferred $e_{1\sigma}$ eigenvectors, respectively, that determine the relative ease of motion of the electronic charge density $\rho(r_b)$.

Suggestions for future work include the exploration of the newly discovered NG-QTAIM bond cross-section set $\{T_\sigma,F_\sigma\}$ for *cis*- and *trans*-isomers, which could be undertaken by manipulating the *cis*- and *trans*-isomer character in U_σ space with laser irradiation. We make this suggestion since NG-QTAIM chirality has already been found to be reversed by the application of an electric field [46]. Reversing the *cis*- and *trans*-isomer character in U_σ space is possible with laser irradiation that is fast enough to avoid disrupting atomic positions. Such a reversal in U_σ space could result in the *cis*- and *trans*-geometric isomers comprising *trans*- and *cis*-isomer assignments in U_σ space, respectively.

Supplementary Materials: The following supporting information can be downloaded at: https://www.mdpi.com/article/10.3390/molecules27186099/s1, S1. NG-QTAIM and stress tensor theoretical background and procedure to generate the stress tensor trajectories $T_\sigma(s)$. S2. Experimental data, geometry optimized structures for ethene, doubly substituted ethene and diazene. S3. Distance measures for ethene, doubly substituted ethene and diazene. S4. Scalar measures (relative energy ΔE) for ethene, doubly substituted ethene and diazene. S5 The maximum stress tensor projections $T_\sigma(s)_{max}$ for ethene, doubly substituted ethene and diazene. S6. Tables of the complete C1-C2 *BCP* U_σ-space distortion sets for ethene and doubly substituted ethene and diazene. References [47–59] are cited in the Supplementary Materials.

Author Contributions: Conceptualization, S.R.K. and S.J.; Data curation, Y.P., W.Y., X.F. and T.X.; Investigation, Y.P., W.Y., X.F., T.X., H.F., T.v.M., S.R.K. and S.J.; Methodology, S.J.; Supervision, S.R.K. and S.J.; Writing—original draft, S.J.; Writing—review and editing, H.F., T.v.M. and S.R.K. All authors have read and agreed to the published version of the manuscript.

Funding: The Hunan Natural Science Foundation of China project approval number: 2022JJ30029. The One Hundred Talents Foundation of Hunan Province is also gratefully acknowledged for the support of S.J. and S.R.K. H.F. and T.v.M. gratefully acknowledge computational support via the EaStCHEM Research Computing Facility.

Institutional Review Board Statement: Not applicable.

Informed Consent Statement: Not applicable.

Data Availability Statement: Not applicable.

Acknowledgments: The Hunan Natural Science Foundation of China is gratefully acknowledged, project approval number: 2022JJ30029. The One Hundred Talents Foundation of Hunan Province is also gratefully acknowledged for the support of S.J. and S.R.K. H.F. and T.v.M. gratefully acknowledge computational support via the EaStCHEM Research Computing Facility.

Conflicts of Interest: The authors declare no conflict of interest.

Sample Availability: Samples of the compounds are available from the authors.

References

1. Garcia-Fernandez, P.; Liu, Y.; Bersuker, I.B.; Boggs, J.E. Pseudo Jahn–Teller Origin of Cis–Trans and Other Conformational Changes. The Role of Double Bonds. *Phys. Chem. Chem. Phys.* **2011**, *13*, 3502–3513. [CrossRef] [PubMed]
2. Feller, D.; Peterson, K.A.; Dixon, D.A. Ab Initio Coupled Cluster Determination of the Heats of Formation of C2H2F2, C2F2, and C2F4. *J. Phys. Chem. A* **2011**, *115*, 1440–1451. [CrossRef] [PubMed]
3. Yamamoto, T.; Kaneno, D.; Tomoda, S. The Origin of Cis Effect in 1,2-Dihaloethenes: The Quantitative Comparison of Electron Delocalizations and Steric Exchange Repulsions. *Bull. Chem. Soc. Jpn.* **2008**, *81*, 1415–1422. [CrossRef]
4. Zhao, D.B.; Rong, C.Y.; Jenkins, S.; Kirk, S.R.; Yin, D.L.; Liu, S.B. Origin of the Cis-Effect: A Density Functional Theory Study of Doubly Substituted Ethylenes. *Acta Phys. Chim. Sin.* **2013**, *29*, 43–54. [CrossRef]
5. Banerjee, D.; Ghosh, A.; Chattopadhyay, S.; Ghosh, P.; Chaudhuri, R.K. Revisiting the ' *Cis*- Effect' in 1,2-Difluoro Derivatives of Ethylene and Diazene Using Ab Initio Multireference Methods. *Mol. Phys.* **2014**, *112*, 3206–3224. [CrossRef]
6. Tavanaei, L.; Nori-Shargh, D. New Insights into the Origin of the Cis-Configuration Preferences in 1,2-Dihaloethenes: The Importance of the Bonding Orbital Deviations. *Aust. J. Chem.* **2018**, *71*, 1–13. [CrossRef]
7. Pasto, D.J.; Trobe, M.; Dobrounig, P.; Breinbauer, R. Potassium Azodicarboxylate. In *Encyclopedia of Reagents for Organic Synthesis*; e-EROS; Wiley: New York, NY, USA, 2001; pp. 1–5. ISBN 978-0-471-93623-7.
8. Craig, N.C.; Piper, L.G.; Wheeler, V.L. Thermodynamics of Cis-Trans Isomerizations. II. 1-Chloro-2-Fluoroethylenes, 1,2-Difluorocyclopropanes, and Related Molecules. *J. Phys. Chem.* **1971**, *75*, 1453–1460. [CrossRef]
9. Craig, N.C.; Entemann, E.A. Thermodynamics of Cis-Trans Isomerizations. The 1,2-Difluoroethylenes. *J. Am. Chem. Soc.* **1961**, *83*, 3047–3050. [CrossRef]
10. Craig, N.C.; Overend, J. Vibrational Assignments and Potential Constants for Cis- and Trans-1,2-Difluoroethylenes and Their Deuterated Modifications. *J. Chem. Phys.* **1969**, *51*, 1127–1142. [CrossRef]
11. Craig, N.C.; Chen, A.; Suh, K.H.; Klee, S.; Mellau, G.C.; Winnewisser, B.P.; Winnewisser, M. Complete Structure of the Anti Rotamer of 1,2-Difluoroethane from High-Resolution Infrared Spectroscopy. *J. Phys. Chem. A* **1997**, *101*, 9302–9308. [CrossRef]
12. Craig, N.C.; Lo, Y.S.; Piper, L.G.; Wheeler, J.C. Vibrational Assignments and Potential Constants for Cis- and Trans-1-Chloro-2-Fluoroethylenes and Their Deuterated Modifications. *J. Phys. Chem.* **1970**, *74*, 1712–1727. [CrossRef]
13. Wood, R.E.; Stevenson, D.P. The Energy of Isomerization of Cis- and Trans-Dichloroethylene. *J. Am. Chem. Soc* **2002**, *63*, 1650–1653. [CrossRef]
14. Gardner, D.V.; McGreer, D.E. Influence of Steric and Polar Effects in Determining the Equilibrium Position for Cis-Trans-Olefin Pairs. *Can. J. Chem.* **1970**, *48*, 2104. [CrossRef]
15. Craig, N.C.; Brandon, D.W.; Stone, S.C.; Lafferty, W.J. Partial Structure for Trans-1,2-Difluoroethylene from High-Resolution Infrared Spectroscopy. *J. Phys. Chem.* **1992**, *96*, 1598–1605. [CrossRef]
16. Waldron, J.T.; Snyder, W.H. Thermodynamics of Cis-Trans Isomerizations. Relative Stabilities of the 1,2-Dimethoxyethylenes. *J. Am. Chem. Soc.* **1973**, *95*, 5491–5495. [CrossRef]
17. Tokuhashi, K.; Uchimaru, T.; Takizawa, K.; Kondo, S. Rate Constants for the Reactions of OH Radicals with the (*E*)/(*Z*) Isomers of CFCl=CFCl and (*E*)-CHF=CHF. *J. Phys. Chem. A* **2019**, *123*, 4834–4843. [CrossRef]
18. Jenkins, S.; Kirk, S.R.; Rong, C.; Yin, D. The Cis-Effect Using the Topology of the Electronic Charge Density. *Mol. Phys.* **2012**, *111*, 1–13. [CrossRef]
19. Kirk, S.R.; Jenkins, S. Beyond Energetic and Scalar Measures: Next Generation Quantum Theory of Atoms in Molecules. *WIREs Computational Molecular Science* **2022**, *Early View*, e1611. [CrossRef]
20. Li, Z.; Xu, T.; Früchtl, H.; van Mourik, T.; Kirk, S.R.; Jenkins, S. Chiral and Steric Effects in Ethane: A next Generation QTAIM Interpretation. *Chem. Phys. Lett.* **2022**, *800*, 139669. [CrossRef]
21. Xu, T.; Nie, X.; Li, S.; Yang, Y.; Früchtl, H.; Mourik, T.; Kirk, S.R.; Paterson, M.J.; Shigeta, Y.; Jenkins, S. Chirality without Stereoisomers: Insight from the Helical Response of Bond Electrons. *ChemPhysChem* **2021**, *22*, 1989–1995. [CrossRef]
22. Xing, H.; Azizi, A.; Momen, R.; Xu, T.; Kirk, S.R.; Jenkins, S. Chirality–Helicity of Cumulenes: A Non-Scalar Charge Density Derived Perspective. *Int. J. Quantum Chem.* **2022**, *122*, e26884. [CrossRef]
23. Hu, M.X.; Xu, T.; Momen, R.; Azizi, A.; Kirk, S.R.; Jenkins, S. The Normal Modes of Vibration of Benzene from the Trajectories of Stress Tensor Eigenvector Projection Space. *Chem. Phys. Lett.* **2017**, *677*, 156–161. [CrossRef]
24. Huang, W.J.; Xu, T.; Kirk, S.R.; Filatov, M.; Jenkins, S. QTAIM and Stress Tensor Bond-Path Framework Sets for the Ground and Excited States of Fulvene. *Chem. Phys. Lett.* **2018**, *713*, 125–131. [CrossRef]
25. Li, J.H.; Huang, W.J.; Xu, T.; Kirk, S.R.; Jenkins, S. Stress Tensor Eigenvector Following with Next-Generation Quantum Theory of Atoms in Molecules. *Int. J. Quantum Chem.* **2018**, *119*, e25847. [CrossRef]
26. Guo, H.; Morales-Bayuelo, A.; Xu, T.; Momen, R.; Wang, L.; Yang, P.; Kirk, S.R.; Jenkins, S. Distinguishing and Quantifying the Torquoselectivity in Competitive Ring-Opening Reactions Using the Stress Tensor and QTAIM. *J. Comput. Chem.* **2016**, *37*, 2722–2733. [CrossRef]

27. Yang, P.; Xu, T.; Momen, R.; Azizi, A.; Kirk, S.R.; Jenkins, S. Fatigue and Photochromism S1 Excited State Reactivity of Diarylethenes from QTAIM and the Stress Tensor. *Int. J. Quantum Chem.* **2018**, *118*, e25565. [CrossRef]
28. Xu, T.; Wang, L.; Ping, Y.; van Mourik, T.; Früchtl, H.; Kirk, S.R.; Jenkins, S. Quinone-Based Switches for Candidate Building Blocks of Molecular Junctions with QTAIM and the Stress Tensor. *Int. J. Quantum Chem.* **2018**, *118*, e25676. [CrossRef]
29. Xu, T.; Farrell, J.; Momen, R.; Azizi, A.; Kirk, S.R.; Jenkins, S.; Wales, D.J. A Stress Tensor Eigenvector Projection Space for the (H2O)5 Potential Energy Surface. *Chem. Phys. Lett.* **2017**, *667*, 25–31. [CrossRef]
30. Bader, R.F.W. Quantum Topology of Molecular Charge Distributions. III. The Mechanics of an Atom in a Molecule. *J. Chem. Phys.* **1980**, *73*, 2871–2883. [CrossRef]
31. Anderson, J.S.M.; Ayers, P.W.; Hernandez, J.I.R. How Ambiguous Is the Local Kinetic Energy?†. *J. Phys. Chem. A* **2010**, *114*, 8884–8895. [CrossRef]
32. Anderson, J.S.M.; Ayers, P.W. Quantum Theory of Atoms in Molecules: Results for the SR-ZORA Hamiltonian. *J. Phys. Chem. A* **2011**, *115*, 13001–13006. [CrossRef] [PubMed]
33. Keith, T.A. AIMAll (19.10.12), TK Gristmill Software, Overland Park KS, USA 2019. Available online: Http://Aim.Tkgristmill.Com (accessed on 9 August 2022).
34. Xu, T.; Kirk, S.R.; Jenkins, S. A Comparison of QTAIM and the Stress Tensor for Chirality-Helicity Equivalence in S and R Stereoisomers. *Chem. Phys. Lett.* **2020**, *738*, 136907. [CrossRef]
35. Szarek, P.; Sueda, Y.; Tachibana, A. Electronic Stress Tensor Description of Chemical Bonds Using Nonclassical Bond Order Concept. *J. Chem. Phys.* **2008**, *129*, 094102. [CrossRef] [PubMed]
36. Lee, T.J.; Taylor, P.R. A Diagnostic for Determining the Quality of Single-Reference Electron Correlation Methods. *Int. J. Quantum Chem.* **1989**, *36*, 199–207. [CrossRef]
37. Hegarty, D.; Robb, M.A. Application of Unitary Group Methods to Configuration Interaction Calculations. *Mol. Phys.* **1979**, *38*, 1795–1812. [CrossRef]
38. Robb, M.A.; Niazi, U. The Unitary Group Approach to Electronic Structure Computations. In *Reports in Molecular Theory*; Weinstein, H., Náray-Szabó, G., Eds.; CRC Press: Boca Raton, FL, USA, 1990; Volume 1, pp. 23–55.
39. Michael, J.F.; Trucks, G.W.; Schlegel, H.B.; Scuseria, G.E.; Robb, M.A.; Cheeseman, J.R.; Scalmani, G.; Barone, V.; Mennucci, B.; Petersson, G.A.; et al. Gaussian 09, Revision E.01 2009.
40. Brémond, É.; Tognetti, V.; Chermette, H.; Sancho-García, J.C.; Joubert, L.; Adamo, C. Electronic Energy and Local Property Errors at QTAIM Critical Points While Climbing Perdew's Ladder of Density-Functional Approximations. *J. Chem. Theory Comput.* **2022**, *18*, 293–308. [CrossRef]
41. Yamamoto, T.; Kaneno, D.; Tomoda, S. The Importance of Lone Pair Delocalizations: Theoretical Investigations on the Stability of Cis and Trans Isomers in 1,2-Halodiazenes. *J. Org. Chem.* **2008**, *73*, 5429–5435. [CrossRef]
42. Schneider, S.; Gerken, M.; Haiges, R.; Schroer, T.; Boatz, J.A.; Dixon, D.A.; Grant, D.J.; Christe, K.O. Synthesis and Characterization of Silyldichloramines, Their Reactions with F- Ions, Instability of N2Cl2 and NCl2-, and Formation of NCl3. *Inorg. Chem.* **2007**, *46*, 93–102. [CrossRef]
43. Kirk, S.R.; Jenkins, S. QuantVec. 2021. Available online: https://zenodo.org/record/5553687#.YybZHrRBxPY (accessed on 9 August 2022).
44. Li, Z.; Xu, T.; Früchtl, H.; van Mourik, T.; Kirk, S.R.; Jenkins, S. Mixed Chiral and Achiral Character in Substituted Ethane: A Next Generation QTAIM Perspective. *Chem. Phys. Lett.* **2022**, *803*, 139762. [CrossRef]
45. Hanson, R.M.; Musacchio, S.; Mayfield, J.W.; Vainio, M.J.; Yerin, A.; Redkin, D. Algorithmic Analysis of Cahn–Ingold–Prelog Rules of Stereochemistry: Proposals for Revised Rules and a Guide for Machine Implementation. *J. Chem. Inf. Model.* **2018**, *58*, 1755–1765. [CrossRef]
46. Li, Z.; Nie, X.; Xu, T.; Li, S.; Yang, Y.; Früchtl, H.; van Mourik, T.; Kirk, S.R.; Paterson, M.J.; Shigeta, Y.; et al. Control of Chirality, Bond Flexing and Anharmonicity in an Electric Field. *Int. J. Quantum Chem.* **2021**, *121*, e26793. [CrossRef]
47. Bader, R.F.W. A Bond Path: A Universal Indicator of Bonded Interactions. *J. Phys. Chem. A* **1998**, *102*, 7314–7323. [CrossRef]
48. Bader, R.F.W. Bond Paths Are Not Chemical Bonds. *J. Phys. Chem. A* **2009**, *113*, 10391–10396. [CrossRef] [PubMed]
49. Nakatsuji, H. Common Nature of the Electron Cloud of a System Undergoing Change in Nuclear Configuration. *J. Am. Chem. Soc.* **1974**, *96*, 24–30. [CrossRef]
50. Bone, R.G.A.; Bader, R.F.W. Identifying and Analyzing Intermolecular Bonding Interactions in van Der Waals Molecules. *J. Phys. Chem.* **1996**, *100*, 10892–10911. [CrossRef]
51. Jenkins, S.; Heggie, M.I. Quantitative Analysis of Bonding in 90° Partial Dislocation in Diamond. *J. Phys. Condens. Matter* **2000**, *12*, 10325–10333. [CrossRef]
52. Ayers, P.W.; Jenkins, S. An Electron-Preceding Perspective on the Deformation of Materials. *J. Chem. Phys.* **2009**, *130*, 154104. [CrossRef] [PubMed]
53. Jenkins, S.; Morrison, I. The Chemical Character of the Intermolecular Bonds of Seven Phases of Ice as Revealed by Ab Initio Calculation of Electron Densities. *Chem. Phys. Lett.* **2000**, *317*, 97–102. [CrossRef]
54. Jenkins, S.; Maza, J.R.; Xu, T.; Jiajun, D.; Kirk, S.R. Biphenyl: A Stress Tensor and Vector-Based Perspective Explored within the Quantum Theory of Atoms in Molecules. *Int. J. Quantum Chem.* **2015**, *115*, 1678–1690. [CrossRef]
55. Wyatt, R.E. *Quantum Dynamics with Trajectories; Interdisciplinary Applied Mathematics*, 1st ed.; Springer: Dordrecht, The Netherlands, 2006; ISBN 978-0-387-28145-2.

56. Xu, T.; Momen, R.; Azizi, A.; van Mourik, T.; Früchtl, H.; Kirk, S.R.; Jenkins, S. The Destabilization of Hydrogen Bonds in an External E-Field for Improved Switch Performance. *J. Comput. Chem.* **2019**, *40*, 1881–1891. [CrossRef] [PubMed]
57. Tian, T.; Xu, T.; van Mourik, T.; Früchtl, H.; Kirk, S.R.; Jenkins, S. Next Generation QTAIM for the Design of Quinone-Based Switches. *Chem. Phys. Lett.* **2019**, *722*, 110–118. [CrossRef]
58. Yang, W.; Zurbenko, I. Kolmogorov–Zurbenko Filters. *WIREs Comp. Stat.* **2010**, *2*, 340–351. [CrossRef]
59. Tian, T.; Xu, T.; Kirk, S.R.; Rongde, I.T.; Tan, Y.B.; Manzhos, S.; Shigeta, Y.; Jenkins, S. Intramolecular Mode Coupling of the Isotopomers of Water: A Non-Scalar Charge Density-Derived Perspective. *Phys. Chem. Chem. Phys.* **2020**, *22*, 2509–2520. [CrossRef] [PubMed]